LASER & PHOTONICS REVIEWS

www.lpr-journal.org

Ultrahigh Quality Microlasers from Controlled Self-Assembly of Ultrathin Colloidal Semiconductor Quantum Wells

Yi Tian Thung, Rui Duan, Emek G. Durmusoglu, Yichen He, Lian Xiao, Calvin Xiu Xian Lee, Wen Siang Lew, Lin Zhang, Hilmi Volkan Demir, and Handong Sun**

Colloidal quantum wells (CQWs) have emerged as a promising class of gain material in various optical feedback configurations. This is due to their unique excitonic features arising from their 1D quantum confinement. However, existing methods for integrating CQW onto microresonators will cause low laser quality due to uneven CQW coating. To overcome this, the use of liquid-interface kinetically driven self-assembly is proposed to coat ultrathin, close-packed layers of colloidal CdSe/$Cd_{1-x}Zn_xS$ core/shell CQWs between 7 and 14 nm onto the surface of silica microsphere cavities. The fabricated CQW-whispering-gallery-mode microlasers possess a commendable high quality (*Q*) factor of 13 000 at room temperature. Stable single-mode lasing output is demonstrated through evanescent field coupling between a CQW-coated microsphere and a thin uncoated microfiber in a 2D-3D microcavity configuration. These promising results highlight the suitability of the liquid-interface kinetically driven self-assembly method for realizing ultrathin CQW-coated microlasers and its high compatibility for integrating colloidal nanocrystals onto complex 3D microstructures for future miniaturized colloidal optoelectronic and photonic applications.

1. Introduction

Since their inception, 2D colloidal quantum wells (CQWs) based on II-VI semiconductor materials with quantum confinement along its vertical direction[1–3] have emerged as outstanding materials for optoelectronic applications.[4–8] They outshine their 0D quantum dots and 1D nanorods counterparts for lasing applications. This is attributed to their unique advantages including reduced Auger recombination (AR),[9,10] suppressed inhomogeneous broadening,[11,12] giant oscillator strength,[12] large gain cross-sections,[9,12–14] high modal coefficients,[15] and low amplified spontaneous emission (ASE), and lasing thresholds.[16–22] Between different classifications of II-VI semiconductor CQWs, heterostructure CQWs consisting of a CdSe core sandwiched between a compositionally graded $Cd_{1-x}Zn_xS$ shell show superb gain properties, through their ultralow threshold of 3 μJ cm^{-2} for the onset of ASE.[20] The improved surface passivation and fine-tuning of carrier distribution by the graded composition shell results in an effective slowing of AR that predominantly causes loss of lasing action, thus making such CQWs an ideal candidate for optical gain.[19,20]

Core/shell CQWs have been extensively used as optical gain media and for colloidal lasing applications, adopting different optical feedback configurations such as Fabry–Perot cavity,[9,18,23–27] distributed feedback cavity,[28] photonic-crystal cavity,[21,29] random lasing cavity,[30] vertical cavity surface emitting laser

Y. T. Thung, R. Duan, E. G. Durmusoglu, L. Xiao, C. X. X. Lee, W. S. Lew, H. V. Demir, H. Sun
Division of Physics and Applied Physics
School of Physical and Mathematical Sciences
Nanyang Technological University
21 Nanyang Link, Singapore 637371, Singapore
E-mail: hvdemir@ntu.edu.sg; hdsun@ntu.edu.sg

Y. T. Thung, E. G. Durmusoglu, H. V. Demir
LUMINOUS! Centre of Excellence for Semiconductor Lighting and Displays
The Photonics Institute
School of Electrical and Electronic Engineering
Nanyang Technological University
Singapore 639798, Singapore

Y. He, L. Zhang
School of Precision Instruments and Optoelectronics Engineering
Tianjin University
Tianjin 300072, China

H. V. Demir
School of Materials Science and Engineering
Nanyang Technological University
Singapore 639798, Singapore

H. V. Demir
Department of Electrical and Electronics Engineering
Department of Physics
UNAM—Institute of Materials Science and Nanotechnology
Bilkent University
Ankara 06800, Turkey

The ORCID identification number(s) for the author(s) of this article can be found under https://doi.org/10.1002/lpor.202200849

DOI: 10.1002/lpor.202200849

 © 2023 Wiley-VCH GmbH

(VCSEL),[31] and whispering-gallery-mode (WGM) cavity.[22,32] In particular, WGM resonators have been claimed to be highly promising cavities for light amplification, owing to their low optical losses, strong optical confinement, and enhanced light-matter interaction.[33–35] The potential and reliability of WGM microlasers are highlighted by the advances they made in the areas of nonlinear optics,[36,37] integrated optics,[38–40] novel coherent light source,[38,39] and ultrahigh-sensitivity sensing.[41–44] Fabricated via reliable and advanced microfabrication techniques, WGM resonators can function in the forms of microrings,[45] microdisks,[46] microfibers,[47–49] and microspheres.[22,50] These are capable of ultrahigh quality (*Q*-) factor, low lasing threshold, and small mode volume.[33–35] Compared to traditional organic dye-based miniaturized lasers suffering from low photostability and irreversible photobleaching, CQW-WGM microlasers see a greater gain in media packing density for improved lasing stability and lower lasing threshold.[33,35,51] Such advantages offer new opportunities in developing high-performance, emission wavelength-tunable future miniaturized lasers.

WGM lasing from CQWs was previously exemplified through a coreless fiber-based CQW-WGM laser,[32] achieving multimode lasing with a threshold up to 188 μJ cm^{-2}, and from CQW-coated microsphere[22] with multimode and single mode lasing thresholds at 3.26 and 3.84 μJ cm^{-2}, respectively. However, these breakthroughs highlighting the novelty and potential of colloidal semiconductor CQWs in miniaturized lasers were far from perfect. The coreless fiber CQW-WGM laser[32] saw significant optical losses, and its preparation was via slowly dipping in highly concentrated CQW dispersion to ensure uniformity and smoothness of the closed-packed CQW film. This coating method is time-consuming, challenging, and costly. The drop-casted CQW-coated microspheres[22] require a significant amount of CQWs to create a close-packed CQW film on the microspheres and results in nonuniform coatings with significant variance in thicknesses, which limits the quality of lasing achieved. As the smoothness of CQW coating on resonators' surfaces is influential on the quality of lasing output, there is a need for alternative methods that ensure smooth and closed-packed CQW coating while not compromising the facility in fabricating CQW-WGM lasers surface as a priority in the area of miniaturized solid-state lasers.

Recently, colloidal self-assembly at liquid interfaces has been utilized for depositing thin, close-packed CQW films with uniform orientation, i.e., either all face-down or all edge-up.[51–57] In this method, control of CQWs' orientation is achieved thermodynamically via tuning the interaction potential between CQWs and subphase during the self-assembly process.[51–57] Previous applications of colloidal self-assembly have seen coatings of closely packed, monolayer-thick 2D superlattice CQW thin films with a grain size of hundreds of micrometers on flat surfaces.[54,55] Face-down CQW superlattices prepared using self-assembly have demonstrated roughness in the range of nanometers.[55] The ability to form thin, smooth films of uniformly oriented CQWs has made possible unique applications such as thickness-controlled CQW superstructures via sequential deposition,[55] single-layer monolithic CQW-VCSEL,[31] and multicolor CQW patterning,[56] which are not possible with randomly oriented CQWs. The improvement in CQW packing density and film smoothness from the self-assembly method opens an avenue to investigate the compatibility of this method in creating thin and smooth CQW coating on 3D resonator structures for boosting the lasing quality of semiconductor CQW microlasers.

Inspired by the advances in CQW self-assembly and WGM lasing, we demonstrate in this work the use of interfacial self-assembly to improve lasing quality of CQW-WGM microlasers. We make use of the kinetically driven liquid–liquid interface self-assembly to coat CdSe/$Cd_{1-x}Zn_xS$ core/alloyed–shell CQWs onto silica microsphere resonators of varying diameters. This allows for the fabrication of CQW-WGM microlasers with ultrathin and smooth CQW coatings with improved lasing quality at room temperature. The microlasers exhibit a high Q-factor of 13 000 and a commendable low lasing threshold of 27.67 μJ cm^{-2} under nanosecond pumping, demonstrating stable lasing output with a mere 6% loss of lasing intensity under strong nanosecond pumping for 120 min. The WGM mechanism is systematically studied via experimental findings, including mode analysis and size-dependent free spectral range. Detailed simulations of electric field profiles within the microspheres indicate novel findings that with thin CQW films coated on microspheres, the WGM lasing occurs inside the resonators, rather than within the CQW material coating. We also demonstrate that through evanescent coupling between a CQW-coated microsphere and uncoated microfiber, single-mode lasing can be obtained. The findings highlight the compatibility of the self-assembly method in creating thin and smooth coatings of CQWs on miniaturized 3D structures. This indicates the greater suitability of the self-assembly method for fabricating functional microlasers with improved lasing performance. The ability of the self-assembly method in overcoming the limitations of previous CQW deposition methods offers insights into how to effectively integrate colloidal CQWs for future miniaturized optoelectronic and photonic applications.

2. Results and Discussions

2.1. CdSe/$Cd_{1-x}Zn_xS$ Core/Alloyed–Shell CQWs

We synthesized zinc blende four monolayers (ML) core CdSe NPLs by referring to a method used in a previous study.[21] These cores were then used in synthesizing CdSe/$Cd_{1-x}Zn_xS$ core/alloyed–shell CQWs via the hot-injection technique with slight modifications from a previous report.[20] Adopting of core/alloyed–shell structure for CQWs has effectively reduced interfacial defects between core and shell components by improving lattice constant matching, suppressing large AR typical of core/shell CQWs by relaxing momentum conservation from the sharp interface potential between core and shell components.[58–60] These modifications boost the photoluminescence quantum yield (PL QY) and ensure a uniformly shaped narrow emission line width[19,20] for further lasing applications. In addition, the strong type-I confinement provided by the $Cd_{1-x}Zn_xS$ alloyed-shell confine photoexcited carriers much better than a pure CdS shell, increasing the overlap of their wavefunctions to prevent excitons from interacting with surface defects and hence resulting in superior gain features.[19,20,61]

The transmission electron microscopy (TEM) image of the CQWs under a bright field is shown in **Figure 1**a. As can be seen, the as-synthesized CQWs possess a square-like lateral shape with a low aspect ratio. This shape has been shown to improve packing density, enhance film morphology, and reduce the surface

© 2023 Wiley-VCH GmbH

18638899, 2023, 7, Downloaded from https://onlinelibrary.wiley.com/doi/10.1002/lpor.202200849 by Bilkent University, Wiley Online Library on [10/07/2023]. See the Terms and Conditions (https://onlinelibrary.wiley.com/terms-and-conditions) on Wiley Online Library for rules of use; OA articles are governed by the applicable Creative Commons License

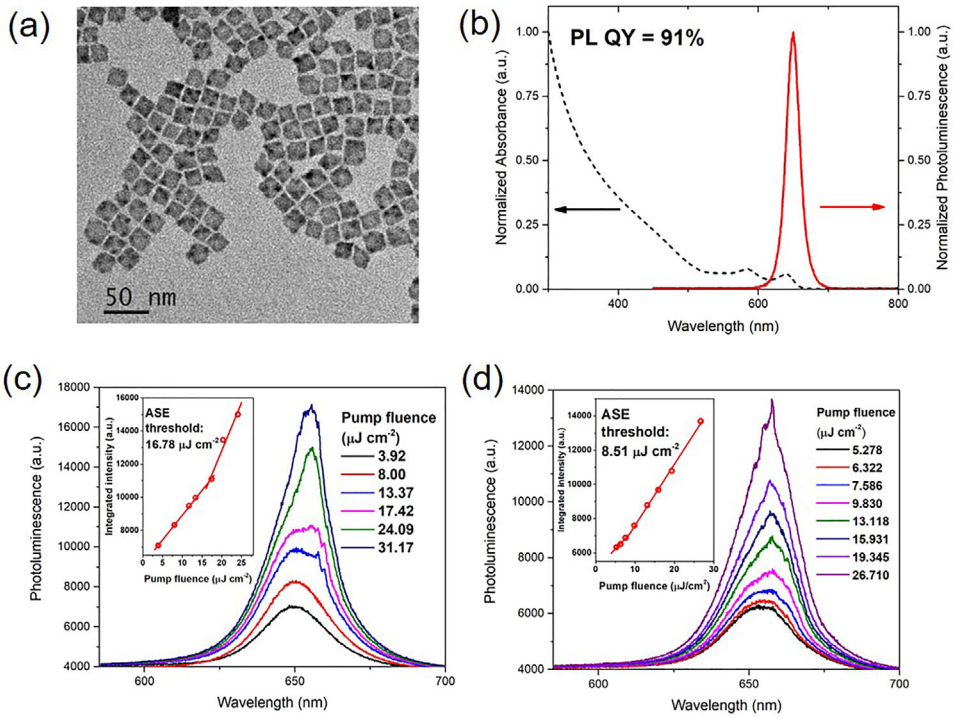

Figure 1. a) Bright-field TEM image of 4 ML CdSe/$Cd_{1-x}Zn_xS$ core/shell CQWs. b) Normalized absorbance and photoluminescence spectra of the as-synthesized core/shell CQWs and its PL QY at room temperature. c) Emission spectra of self-assembled CQWs film using a hexane solution of OD 0.13, under femtosecond pulse excitation with increasing pump fluence. Inset shows the integrated edge emission intensity as a function of pump fluence. d) Emission spectra of self-assembled CQWs film using a hexane solution of OD 0.25, under femtosecond pulse excitation with increasing pump fluence. Inset shows the integrated edge emission intensity as a function of pump fluence.

roughness of CQW thin films in optoelectronic applications.[7] Figure 1b depicts the absorbance and photoluminescence (PL) spectra of the CQWs. Note that heavy- and light-hole excitonic transitions are well-resolved at 639.5, and at 583 nm, and the PL emission at 649.5 nm has a narrow full width at half maximum (FWHM) of 21 nm. The high PL QY of 91% measured from the as-synthesized CQWs is also in tandem with results from previous reports of core/alloyed–shell CQWs.[7,19,20,22]

To evaluate the gain properties of core/alloyed–shell CQWs, we prepared thin films via the kinetically driven self-assembly method modified from Momper et al.[57] for ASE measurements under femtosecond laser pumping. Surface profiling from Figure S3b (Supporting Information) shows that a single layer of face-down CQW is deposited as a thin film, with surface roughness at 3.2 nm. Pump fluence-dependent integrated emission intensity of a CQW thin film prepared with CQW hexane solution of optical density (OD) of 0.13 from Figure 1c indicates ASE threshold $P_{th} \approx 16.78$ μJ cm^{-2}, with a redshift of the PL emission peak with increasing pump fluence indicating onset of ASE. For the thin film formed from a higher concentrated CQW solution at OD 0.25, Figure 1d shows ASE threshold $P_{th} \approx 8.51$ μJ cm^{-2} and a more prominent appearance of a narrower emission band to the right of the spontaneous emission band. The ASE from these self-assembled CQW thin films indicates a multiexcitonic gain mechanism within the as-synthesized core/alloyed–shell CQWs.[9,18,19,23,27] These results indicate the suitability of core/alloyed–shell CQWs for lasing applications, and the observation of optical gain from CQW thin films prepared via interfacial self-assembly indicates the feasibility of employing this method to boost lasing performance in CQW-WGM microlasers.

2.2. Self-Assembly Mechanism and Fabrication of CQW-WGM Microsphere Laser

Self-assembly of CQWs at the interface has shown to be a convenient and versatile method to control the orientation of CQWs, allowing the fabrication of highly ordered superlattices for use in functional optoelectronic and optical gain applications. CQWs can be assembled into ordered superlattices by influencing the interaction potential at the interface, via methods such as the use of additives,[51] choice of polar subphase,[53–56] or kinetic control through varying CQW solvent evaporate rate.[57] Supported by a previous demonstration[55] and results obtained from atomic force microscopy (AFM) (see Figure S3, Supporting Information), it is evident that the interfacial self-assembly method overcomes issues of surface roughness and nonuniformity of CQW coating thickness, which are common in drop-casting[22] and solution-dipping.[32] Addressing these issues is essential for fabricating CQW-WGM microlasers with improved lasing quality.

To retain the benefits of previous preparation methods, such as facile fabrication and the ability to create closely packed CQW films, Momper et al.'s kinetically driven self-assembly method[57] appears to be the most superior. By varying temperature, choice of subphase, and alkane vapor content to influence

© 2023 Wiley-VCH GmbH

18638899, 2023, 7, Downloaded from https://onlinelibrary.wiley.com/doi/10.1002/lpor.202200849 by Bilkent University, Wiley Online Library on [10/07/2023]. See the Terms and Conditions (https://onlinelibrary.wiley.com/terms-and-conditions) on Wiley Online Library for rules of use; OA articles are governed by the applicable Creative Commons License

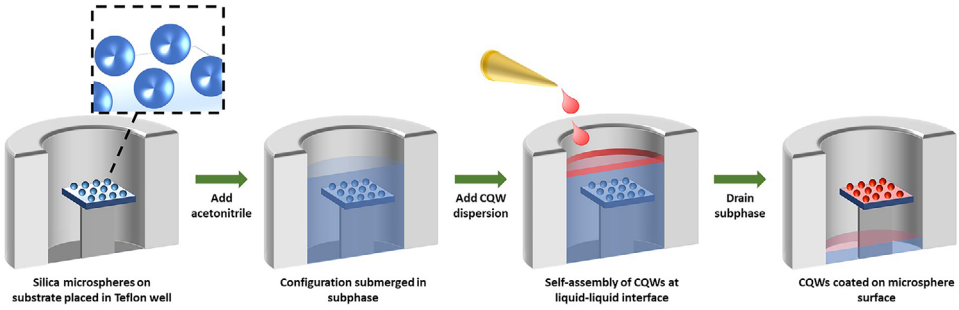

Figure 2. Step-by-step schematics for the fabrication of thinly coated CQW-WGM microlasers employing SiO_2 microspheres as a resonant cavity. Kinetically driven liquid–liquid interface self-assembly is adopted to coat a thin layer of CQWs in face-down orientation uniformly on the microspheres' surface.

CQWs' solvent evaporation rate at liquid interfaces, Momper et al. demonstrate the ability to obtain an ensemble of four ML core CdSe CQWs in collective face-down long-range orientation within minutes. The method avoids using insulating additives and requires only facile preparation. It is thus clearly most suitable for coating CQWs onto micro 3D structures for our desired CQW-WGM microlasers.

In this work, we prepare CQW-WGM microlasers with modifications to the typical kinetically driven self-assembly deposition[57] of CQWs under ambient conditions and room temperature, with procedures illustrated in **Figure 2**. To minimize the amount of CQWs employed for a maximal surface area coverage of microspheres, we sought to deposit CQWs in a face-down orientation. We first dispersed silica microspheres in an ethanol solution were first dispersed onto a square-shaped precleaned glass, silica wafer, or double Bragg reflector (DBR) substrates, before placing the configuration within a Teflon well. We then added acetonitrile into the well as the subphase until the microsphere configuration is fully submerged. Subsequently, we added 50 µL of a hexane solution of CdSe/$Cd_{1-x}Zn_xS$ core/alloyed–shell CQWs dropwise in quick succession onto the subphase surface.

As acetonitrile has a higher density than hexane and a moderate polarity index of 0.460,[61] added CQWs spread over the acetonitrile surface. The polarity of acetonitrile assures immiscibility with the CQWs, and also results in a high interaction potential with the CQWs to assemble them in a face-down orientation. The quick evaporation of hexane under ambient conditions prevents CQWs from stacking in an edge-up configuration. After complete evaporation of hexane, the subphase is slowly drained through a needle, transferring a closely packed, uniformly oriented CQW thin film onto the surface of the silica microspheres to produce thinly coated CQW-WGM microlasers.

Figure 3a illustrates WGM lasing under optical pumping produced from a CQW-coated silica microsphere resonator. As can be seen from the scanning electron microscope (SEM) images of Figure 3b–d, the sphericity of microspheres is maintained after the conformal coating of CQWs on the microspheres via self-assembly. The comparison of microsphere surface morphology before and after CQW coating indicates that the microsphere's smooth surface is preserved throughout the self-assembly coating process. These observations are in tandem with demonstrations from previous CQW self-assembly works, which formed closely packed CQW membranes with smooth surfaces on flat substrates.[55,57]

The distribution of CQWs coated on microsphere resonators can be examined through energy dispersive spectrometer (EDS) mapping in Figure 3e–j. The intensity of EDS mapping indicates that a minimal amount of CQWs was deposited on the microsphere and was uniformly distributed across the microsphere's surface. These observations show that the self-assembly method is capable of fabricating thinly coated CQW-WGM microsphere lasers with a uniform CQW coverage. This is in agreement with our AFM results shown in Figure S3 (Supporting Information), where surface profiling studies show that the self-assembly method is capable of depositing CQW coatings consisting of between one to two layers of CQWs, approximately between 7 and 14 nm. The combination of smooth morphology, uniform distribution, close packing, and a thin coating of CQW gain medium on the microsphere resonators alleviate scattering losses during lasing operation, resulting in high-quality, low-threshold microlasers. These findings demonstrate the compatibility of the self-assembly method for depositing thinly coated, closely packed CQWs onto 3D microcavities to fabricate miniaturized semiconductor lasers.

2.3. WGM Multimode Lasing

We investigated lasing output from the fabricated CQW-WGM microlasers via a homebuilt microphotoluminescence (µ-PL) system employing nanosecond pulsed laser excitation at 532 nm (1 ns, repetition rate 60 Hz, see Figure S2, Supporting Information). **Figure 4** depicts a spectral examination of WGM lasing produced from a CQW-coated microsphere of diameter ≈40 µm, dispersed on a DBR substrate. Figure 4a shows that spontaneous PL emission with a broad linewidth centered around ≈650 nm was obtained at low pump fluence, and under increasing pump fluence, the PL emission first redshifts to a narrow peak centered around 656 nm and subsequently culminates in sharp lasing spikes of regular intervals and rapidly boosted intensity at higher pump fluence, indicating the onset of multimode lasing. Figure 4b shows the relation between PL intensity and emission linewidth with pump fluence, where a simultaneous rapid decrease of FWHM and sharp increase of PL intensity indicates prominent threshold behavior, confirming the presence of lasing output with a threshold of 27.67 µJ cm^{-2}. Close-up spectral analysis of the multimode lasing profile from a 215 µm diameter microlaser in Figure 4c with calculations from the FWHM

© 2023 Wiley-VCH GmbH

18638899, 2023, 7, Downloaded from https://onlinelibrary.wiley.com/doi/10.1002/lpor.202200849 by Bilkent University, Wiley Online Library on [10/07/2023]. See the Terms and Conditions (https://onlinelibrary.wiley.com/terms-and-conditions) on Wiley Online Library for rules of use; OA articles are governed by the applicable Creative Commons License

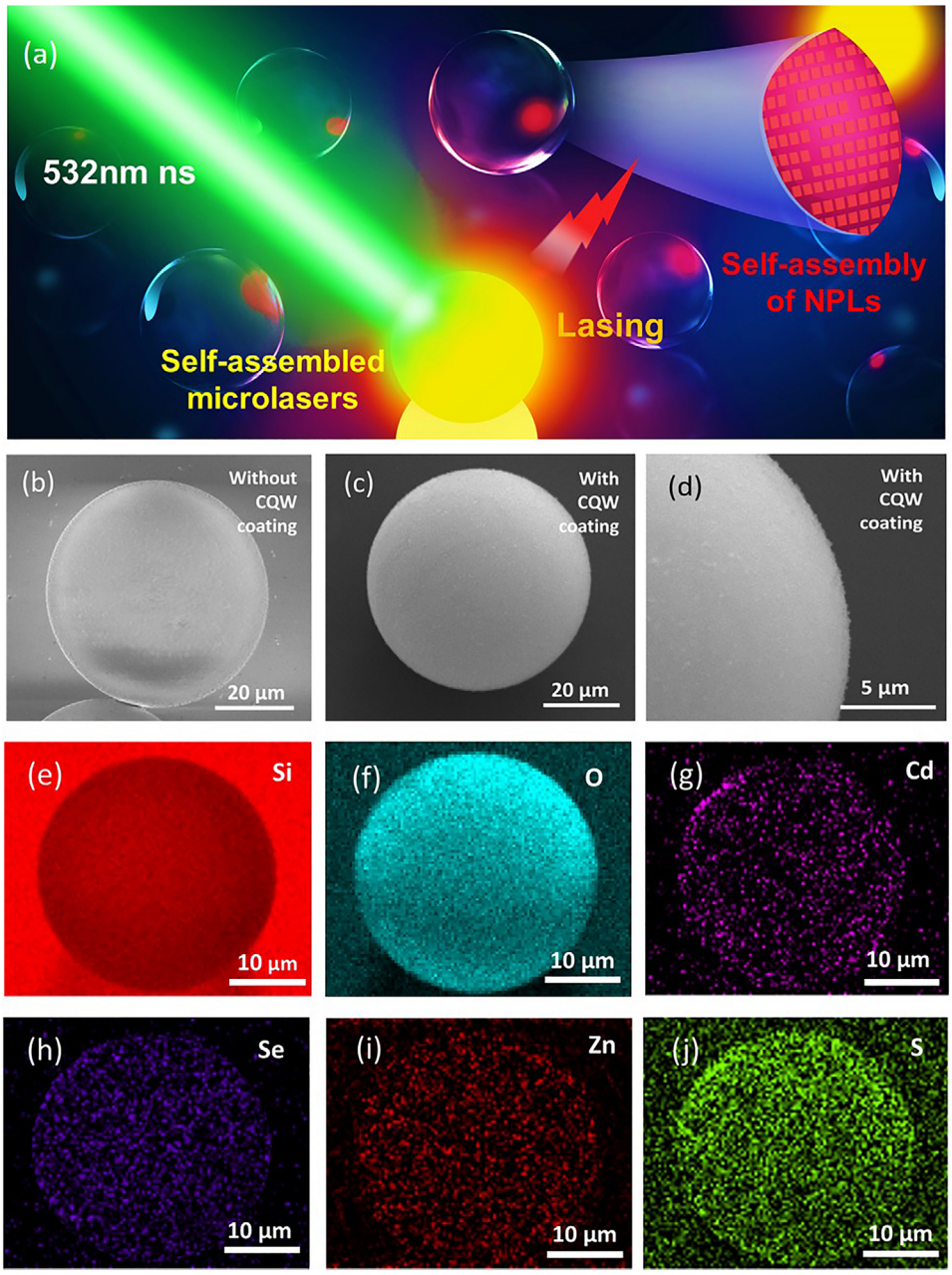

Figure 3. a) Illustration of a CQW-WGM microlaser with CdSe/$Cd_{1-x}Zn_xS$ core/shell CQWs uniformly coated on the microsphere cavity's surface, optically pumped by a nanosecond pulse of 532 nm. b–d) SEM images of bare SiO_2 microsphere, CQW-coated SiO_2 microsphere, and close-up image of a SiO_2 microsphere's surface after CQW coating, respectively. e–j) EDS elemental mapping results depict the distribution of chemical elements around a CQW-coated microsphere.

measured indicates a high *Q*-factor of 13 000, the highest for WGM microlasers employing CQWs as gain media at the time of writing. To verify the development of lasing, we investigate the PL dynamics of the CQW-coated microspheres as a function of pump intensity (Figure S4, Supporting Information). At pump intensity lower than the threshold value, the PL decay gives a spontaneous emission trace. Exciting with pump intensity above the threshold results in the onset of a much faster decay channel, indicating the achievement of optical gain. Compared to our previous demonstration with a record-low threshold of 3.26 µJ cm^{-2},[22] the increased lasing threshold in this work points towards a higher mode volume $V_{\text{eff}} = \frac{\text{Stored energy}}{\text{Max energy density}}$, which is directly proportional to the threshold.[35,62] We speculate that a thinner coating of CQW gain media on the microspheres reduces the maximum energy density of lasing modes, and a higher pump fluence is necessary to induce lasing action.[62]

Compared to our previous work,[22] the improved *Q*-factor of the fabricated microlasers in this work stems from lower optical loss and higher optical confinement. For a spherical resonator,

© 2023 Wiley-VCH GmbH

18638899, 2023, 7, Downloaded from https://onlinelibrary.wiley.com/doi/10.1002/lpor.202200849 by Bilkent University, Wiley Online Library on [10/07/2023]. See the Terms and Conditions (https://onlinelibrary.wiley.com/terms-and-conditions) on Wiley Online Library for rules of use; OA articles are governed by the applicable Creative Commons License

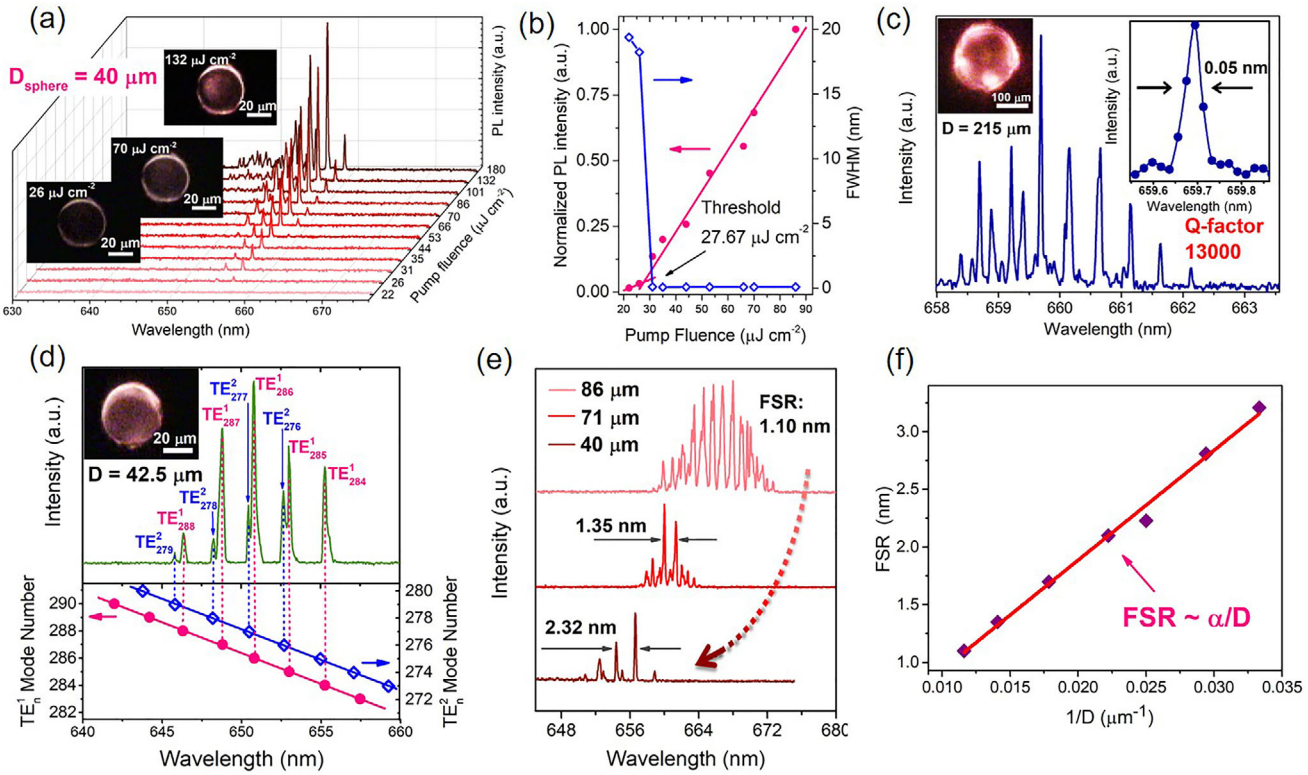

Figure 4. a) Pump-dependent PL emission spectra of a 20 μm diameter CQW-WGM microlaser under nanosecond excitation. The inset depicts microscope photographs of the microlaser at specific pump fluence. The prominent ring on the circumference of the microlaser indicates WGM multimode lasing output. b) Scheme of normalized PL intensity and FWHM of emission peaks as a function of pump fluence of the 20 μm diameter microlaser. c) PL emission spectrum of a 215 μm diameter CQW-WGM microlaser. Calculations from a lasing peak centered around 659.7 nm with a FWHM of 0.05 nm as shown in the inset, gives a *Q*-factor of 13 000. d) Mode analysis of the lasing spectrum from a CQW-WGM microlaser of 42.5 μm diameter. e) Comparison of lasing spectra and FSR from microlasers with diameters of 86, 71, and 40 μm, respectively. f) FSR as a function of the inverse of microlasers' diameters, indicating a linear relationship.

the intrinsic *Q*-factor Q_{int} affected by different losses can be expressed as[62]

$$Q_{int}^{-1} = Q_{mat}^{-1} + Q_{surf}^{-1} + Q_{scatt}^{-1} + Q_{bend}^{-1} \quad (1)$$

Where Q_{mat}^{-1} describes intrinsic material absorption by the CQWs, Q_{surf}^{-1} surface absorption losses, Q_{scatt}^{-1} scattering losses and Q_{bend}^{-1} bending loss from incomplete total internal reflection within the spherical resonator. Analysis of the *Q*-factor calculated with experimental results observed in Figure 2 indicates that various types of losses have been effectively mitigated by adopting the self-assembly method for coating CQWs. The deposition of CQWs in a single, uniformed face-down orientation on the microspheres' surfaces prevents lateral stacking of CQWs, which have previously been shown to induce inter-CQW absorption and nonradiative energy transfer (NRET)[26,63,64] to reduce photoluminescence and lasing output, hence sufficiently reducing Q_{surf}^{-1}. It can be inferred from Figure 3b–d that the preservation of resonator sphericity before and after CQW deposition ensures total internal reflection of lasing output within the microspheres to reduce Q_{bend}^{-1}. We also theorized that the self-assembled CQW-WGM microlasers suffer from scattering losses to a lesser degree when compared to drop-casted CQW-WGM microlasers. The thin coating of CQWs uniformly distributed on a microsphere, as seen in Figure 3b–j, reduces surface roughness and imperfections that are more likely to be created from drop-casting, thus minimizing Q_{scatt}^{-1}. Despite the higher lasing threshold, the improvement in *Q*-factor highlighted the reliability and robustness of the facile self-assembly method for CQW deposition on 3D microcavities. When comparing the results from this work and a previous experiment employing the self-assembled CQWs in a monolithic cavity,[32] the higher *Q*-factor achieved in this work and greater ease of device fabrication indicates better suitability of the self-assembly method for fabricating miniaturized lasers than large-sized devices. This indicates the potential of the self-assembly method in future CQW miniaturized device applications.

To affirm the WGM nature of lasing output from our fabricated microlasers, we further examined their spectral characteristics by analyzing transverse magnetic (TM) or transverse electric (TE) modes from the lasing peaks using an asymptotic equation[51,65,66] (Supporting Information S3). By characterizing the output spectrum from a microsphere of 42.5 μm diameter in Figure 4d, we found good agreement between experimentally measured and fitted results of laser node positions. This confirmed the WGM lasing mechanism in our CQW-coated microspheres. Our theoretical calculations derive the lasing peaks to be of the first ($q = 1$) and second ($q = 2$) order of the TE mode,

© 2023 Wiley-VCH GmbH

18638899, 2023, 7, Downloaded from https://onlinelibrary.wiley.com/doi/10.1002/lpor.202200849 by Bilkent University, Wiley Online Library on [10/07/2023]. See the Terms and Conditions (https://onlinelibrary.wiley.com/terms-and-conditions) on Wiley Online Library for rules of use; OA articles are governed by the applicable Creative Commons License

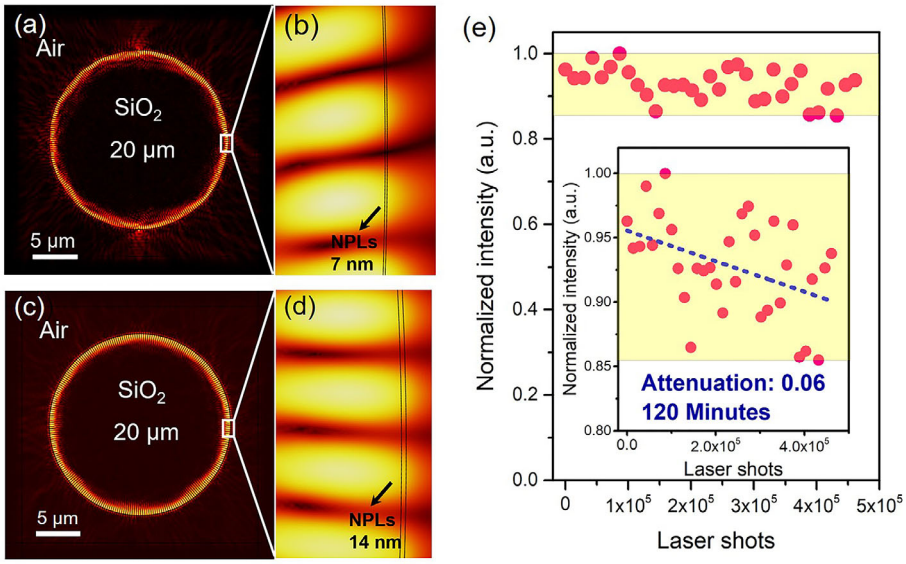

Figure 5. FEM simulations of electric field distribution on the x-y plane of a 20 μm diameter microlaser with a) one layer and c) two layers of CQWs coated on its surface, respectively. Magnified views of the electric field profiles of a) and c) are shown in (b) and (d), respectively. e) Normalized PL intensity under continuous nanosecond excitation of ≈10 times higher than the lasing threshold for 120 min. A linear fitting between relative lasing intensity and laser shots is performed to account for fluctuations due to the instability of the nanosecond excitation source.

with mode numbers counting from 284 to 288 for $q = 1$ peaks and 276 to 279 for $q = 2$ peaks. With lasing emitting radially from the microsphere, the TE modes observed indicate that the electric field oscillates along the surface of the microsphere. Since the dipole moments of CQWs are oriented along their plane, the results in Figure 4d affirm the face-down deposition of CQWs onto the microspheres. Analysis of the free spectral range (FSR) of lasing spectra can further verify the WGM lasing mechanism in the CQW-coated microlasers. The FSR for a spherical resonator is size-dependent and can be represented as[35,51,62]

$$FSR = \lambda^2 / \left(n_{\text{eff}} \pi D\right) \tag{2}$$

where λ, n_{eff}, and D represents the peak wavelength, effective refractive index, and microsphere laser diameter, respectively. A collection of lasing spectra from microspheres of varying diameters is depicted in Figure 4e, showing an increment of FSR calculated from Equation (2) with the reduction in diameter. From Equation (2), the inverse relationship between FSR and D translates as a direct proportion of FSR with $1/D$. The plotting of FSR against $1/D$ in Figure 4f indicates a linear relationship, which coincides with our understanding of Equation (2) to affirm the WGM nature of the CQW-coated microlasers.

Further calculations of experimental results in Figure 4f derive the value of n_{eff} as about 1.47, which is in close agreement with the refractive index of SiO_2 at $n_{SiO_2} = 1.45$. The comparable values between the refractive indices of the CQW-WGM microlasers and bulk SiO_2 suggest that the thin CQW coating makes an insignificant contribution to the overall refractive index of the spherical microlaser configuration, given that the CQWs themselves have a much higher refractive index.[22,55] We explore this understanding by numerically simulating the electric field distribution in the fabricated CQW-WGM microlasers via the finite element method (FEM) using COMSOL Multiphysics in **Figure 5**, with simulation parameters considering experimental measurements and observations, on a microlaser of 20 μm diameter. From Figure 5a,c, simulation results demonstrate that depositing a single layer of CQW gain material of 7 nm on the microsphere's surface is sufficient to support WGM lasing generation, effectively confining light within the resonant cavity via total internal reflection. Together with simulations of microspheres on which surfaces have increased numbers of CQW layers coated in Figure 5b,d, the WGM electric fields generated predominantly occur within the SiO_2 spheres, rather than within the thin CQW coatings. Such simulation results help to explain the closeness between n_{eff} and n_{SiO_2}, and partially for the high Q-factor achieved in this work. With the WGM electric field propagating within the microsphere resonators rather than the CQW coating, it is less likely to interact with potential defects or contaminants present within the CQW coating which may be added during the fabrication process to affect the quality of lasing. The simulations in Figure 5 also indicate minor leakage of WGM electric fields through evanescent waves into the surrounding air, explaining the small discrepancy between n_{eff} and n_{SiO_2}. This analysis further affirms the reliability of the self-assembly method to deposit thin CQW coatings on the surface of microspheres capable of inducing lasing.

In studying the polarization state of lasing behavior, we examined the lasing emission spectra as a function of rotation angle θ of a linear polarizer at a fixed pump intensity above the threshold. Figure S8 (Supporting Information) reveals a strong polarization dependence of the lasing from the fabricated CQW-WGM microlasers. The polarization state factor[67] R is determined to be 0.88, surpassing that from CQW microlasers prepared via solution-dipping[32] and drop-casting[22] methods in previous works (Supporting Information S4). This reflects the superiority of the kinetically-driven self-assembly method in preparing high-quality CQW-WGM microlasers.

© 2023 Wiley-VCH GmbH

18638899, 2023, 7, Downloaded from https://onlinelibrary.wiley.com/doi/10.1002/lpor.202200849 by Bilkent University, Wiley Online Library on [10/07/2023]. See the Terms and Conditions (https://onlinelibrary.wiley.com/terms-and-conditions) on Wiley Online Library for rules of use; OA articles are governed by the applicable Creative Commons License

Benefitting from the superb optical properties of the core/shell CQWs employed and the robustness of the self-assembly fabrication method, our CQW-WGM microlasers exhibit stable lasing output for a prolonged duration. Figure 5e shows the evolution of lasing intensity of a CQW-WGM microlaser under strong, continuous nanosecond pumping at room temperature in an ambient environment for 120 min, with pump fluence of at least one magnitude higher than the lasing threshold. The absence of significant lasing output quenching or chemical degradation is evident from the minor decrease (lesser than 6%) in lasing intensity. The improved lasing stability exemplified in this work compared to our previous demonstration.[22] We attribute the improved lasing stability in this work to WGM electric fields propagating within the SiO_2 microsphere, as opposed to traveling within the deposited CQW coating in our previous work,[22] as simulated in Figure 5a–d. This minimizes opportunities for interaction with surface defects and impurities to reduce long-term lasing intensity. Such excellent results further highlight the suitability of the self-assembly method in integrating core/shell CQWs for reliable, facile, and high-performance WGM lasers, paving a novel direction for miniaturized laser fabrications.

2.4. WGM Single-Mode Lasing

Single-mode lasing is highly desirable for practical applications of miniaturized lasers in areas such as optical fiber communication, optical sensing, and optical information processing. As such, it emerges as a prioritized pursuit in past efforts on semiconductor miniaturized lasers.[68–70] Effective realization of single-mode lasing necessitates the suppression of all but one lasing mode number. Conventionally, this can be realized by increasing the microcavity's FSR to exceed the PL range of gain materials by reducing its size until a single mode remains in the whole gain range, as reflected by Equation (2). Such an approach is unrealistic as there is only a finite limit to which the cavity size can be reduced practically, and further reduction of cavity size could introduce defects on the cavity surface, which worsens the *Q*-factor, following Equation (1), leading to high optical loss. Single-mode lasing can be obtained successfully from coupled WGM cavities via evanescent field coupling. Under this phenomenon, resonance modes circulating in each resonator can interact with one another, whereby one cavity can act as a spectral filter to the resonance wavelengths of the other one under strong interaction. This will enhance certain resonance modes when fulfilling resonance conditions from both cavities while suppressing other modes, which can be exploited to produce the desired single mode lasing.[47,71,72]

Numerous cavities exploiting evanescent field coupling for single-mode lasing have been demonstrated in previous works, such as coupled polymer microfiber cavities,[47,73-75] coupled microspheres,[22] folded nanowires,[74] which adopted similar microcavities as both gain and loss channels. In this work, we demonstrate, that single-mode lasing from CQWs can also be obtained using a hybrid configuration employing different microcavities for gain and loss channels. We adopt a flexible 2D-3D microcavity configuration inspired by Ge et al.'s work,[76] with a 3D CQW-coated microsphere cavity acting as a gain cavity to provide multiple lasing modes, while an uncoated 2D microfiber in the proximity of the microsphere functions as a loss channel to suppress most of the lasing modes, as depicted in **Figure 6**a. Our preparation of the 2D-3D microcavity follows procedures depicted in Figure 2a upon a DBR substrate, with the microfiber added to the substrate after coating the silica microspheres with CQWs. We examined the feasibility of single-mode lasing from the hybrid microcavity configuration using the μ-PL system used to characterize multimode lasing of individual CQW-coated microspheres. Figure 6b shows the typical multimode lasing spectrum from an isolated CQW-coated microsphere cavity of 42 μm diameter, which transforms into single mode lasing after the addition of a 48 μm diameter microfiber, depicted in Figure 6c. It can be observed that single-mode lasing peak centers around 648 nm, showing no redshift of PL emission spectra as pump fluence increases from 34 to 132 μJ cm^{-2}. From Figure 6d, the simultaneous sharp drop in FWHM along with a rapid rise in normalized PL intensity at increasing pump fluence indicates the threshold for stable single mode lasing 45.92 μJ cm^{-2}. These results exemplify the robustness, stability, and suitability of colloidal core/shell CQWs as a gain media for single mode WGM lasing via coupling, achieved by their integration in a novel 2D-3D microcavity with a low lasing threshold, producing stable single-mode lasing peaks over a range of pump fluence up to 132 μJ cm^{-2}, nearly three times of the threshold.

To further understand the coupling process between the CQW-coated microsphere and uncoated microfiber in the hybrid microcavity configuration, we carried out a 3D finite difference time domain (FDTD) numerical simulation to explore the optical field distribution in the configuration. Referring to the axes in Figure 6a, simulations along the *xy*, *yz*, and *xz* planes (see Figure S9, Supporting Information) of the microcavity configuration are shown in Figure 6e,f, with the diameters of the microsphere and fiber resized to 2.1 and 2.4 μm, respectively, for the ease of running simulations on a personal computer. For the resonant mode at $\lambda = 648$ nm, electric field patterns from the CQW-coated microsphere are confined within its inner diameter, analogous to the FEM simulations as depicted in Figure 5a–d. Resonant patterns appear in the microfiber, indicating optical field interaction between the microsphere and microfiber to transfer energy from the microsphere to the microfiber via evanescent coupling. Through comparisons of optical field distribution in Figure 6e,f, the resonant patterns from both microsphere and microfiber are confined within the inner diameter of the cavities, indicating that the uncoated microfiber is attenuating energy density from the CQW-coated microsphere to function as a spectral filter to the resonance wavelengths from the microsphere. This suppresses all but one lasing mode to produce single mode-lasing output from the microsphere. Confinement of resonant patterns within the CQW-coated microsphere from Figure 6e,f also points to a lower possibility for the interaction of electric fields with surface defects introduced during fabrication to result in lasing loss or affect lasing quality. This explains the low lasing threshold observed and the *Q*-factor between 5720 and 7340 achieved.

3. Conclusion

In summary, we demonstrated in this work the facile fabrication of CQW-WGM microlasers using a cost-effective, kinetically driven liquid–liquid interface self-assembly method for coating a

© 2023 Wiley-VCH GmbH

18638899, 2023, 7, Downloaded from https://onlinelibrary.wiley.com/doi/10.1002/lpor.202200849 by Bilkent University, Wiley Online Library on [10/07/2023]. See the Terms and Conditions (https://onlinelibrary.wiley.com/terms-and-conditions) on Wiley Online Library for rules of use; OA articles are governed by the applicable Creative Commons License

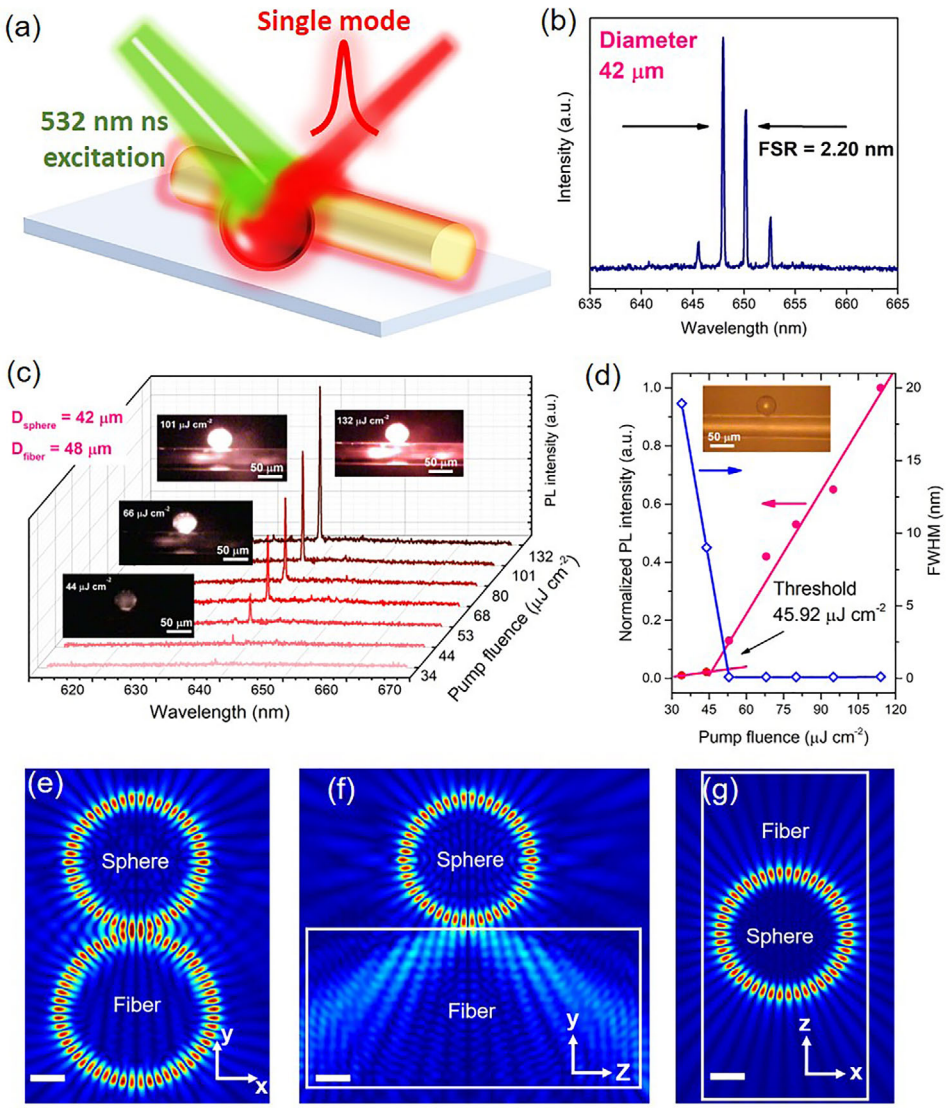

Figure 6. a) Illustration of single mode lasing from a CQW-coated microsphere and uncoated core microfiber in a 2D-3D microcavity configuration due to coupling. b) PL emission spectrum from a single CQW-coated microsphere with a 42 μm diameter indicates multimode lasing. c) Pump-dependent PL emission spectra of a 2D-3D microcavity configuration consisting of the microsphere from b as a gain channel, and a 48 μm diameter microfiber as a loss channel, under nanosecond excitation. Inset depicts microscope photographs of the configuration at various excitation power. d) Normalized PL intensity and FWHM of single mode lasing peaks from the 2D-3D configuration as a function of pump fluence. Inset shows a microscope photograph of the configuration. e–g) FDTD simulations of optical field distribution within the 2D-3D microcavity configuration along the x-y plane, y-z plane, and x-z plane, respectively.

thin layer of CQWs onto the surface of silica microsphere cavities, using low volumes of a dilute hexane solution of core/shell CQWs. The fabricated microsphere lasers exemplified reliable and stable multimode lasing, with a low threshold of 27.67 μJ cm^{-2}, a high *Q*-factor of 13 000, and a mere 6% reduction of lasing intensity under continuous high-intensity nanosecond laser pulse pumping for 120 min. Spectroscopic studies of size-dependent lasing features affirm that the thinly coated microspheres are capable of WGM lasing. These are in good agreement with numerical calculations of transverse electric modes, and along with numerical simulations, affirm that WGM lasing occurs within the silica microsphere cavities to minimize interactions with surface defects that can reduce lasing quality. Demonstration of single-mode lasing is also exemplified through the evanescent field coupling, where a CQW-coated microsphere acts as a gain channel while an uncoated core microfiber functions as a loss channel in a 2D-3D microcavity configuration. Our work offers insights into the reliability and cost-effectiveness of the kinetically driven liquid–liquid interface self-assembly method for coating colloidal CQWs on complex 3D structures for photonic and optoelectronics applications. It contributes to further the understanding of employing colloidal nanomaterials as gain media in fabricating high-quality miniaturized lasers covering the visible spectrum.

© 2023 Wiley-VCH GmbH

18638899, 2023, 7, Downloaded from https://onlinelibrary.wiley.com/doi/10.1002/lpor.202200849 by Bilkent University, Wiley Online Library on [10/07/2023]. See the Terms and Conditions (https://onlinelibrary.wiley.com/terms-and-conditions) on Wiley Online Library for rules of use; OA articles are governed by the applicable Creative Commons License

4. Experimental Section

Synthesis of Colloidal 4ML CdSe/$Cd_{1-x}Zn_xS$ Core/Alloyed–Shell CQWs: The red-emitting core/alloyed–shell CQWs employed in this work were synthesized via the hot-injection method with slight modifications from a previous literature,[20] making use of 4ML core CdSe CQWs synthesized following protocols from a previous study.[21] Detailed synthetic information can be found in the Supporting Information.

Fabrication of CQW-Coated WGM Microsphere Laser and 2D-3D Microcavity Configuration of CQW-Coated Microsphere and Uncoated Core Microfiber: The fabrication process follows procedures modified from previous literature.[52,57] To fabricate the CQW-coated WGM microsphere laser, a DBR substrate of dimensions 1×1 cm^2 was first ultrasonically cleaned in acetone solution for 30 min to remove organic stains on the surface and then blown dry under a nitrogen airflow for 5 min. Subsequently, 10 mg of silica microspheres were dispersed in 100 mL of ethanol and ultrasonically cleaned for 30 min. 50 µL of the microsphere-ethanol dispersion was then dispersed upon the cleaned DBR substrate then dried under ambient conditions for 30 min to ensure complete evaporation of ethanol. The microsphere-substrate configuration was then placed onto a raised stage of 0.5 cm in height and 1 cm in diameter within a Teflon well with an inner diameter of 3 cm, an outer diameter of 5 cm, and a depth of 3.8 cm. After that, ≈8 mL of acetonitrile was added into the Teflon well, submerging the microsphere-substrate configuration within the liquid subphase. 50 µL of $CdSe/Cd_{1-x}Zn_xS$ core/alloyed–shell CQWs in a hexane solution were then added dropwise quickly onto the subphase surface. The hexane solution was then allowed to evaporate for 10 min, after which the subphase was slowly drained through a small hole at the side of the well via a syringe to deposit the CQW membrane upon the surface of the microspheres. During draining, a UV lamp of 345 mm was used to observe the formed membrane. The microsphere-substrate configuration was then allowed to dry under ambient conditions for evaporation of remaining acetonitrile before subsequent lasing characterization. The 2D-3D microcavity configuration is fabricated similar to the microsphere-substrate mentioned above, with the additional step of placing an uncoated core microfiber upon the microsphere-substrate configuration after the complete evaporation of acetonitrile from the configuration.

Simulations for Electromagnetic Field Distribution within CQW-WGM Microsphere Cavity and 2D-3D Microcavity Coupling Configuration: The behavior and distribution of the electric field within the CQW-coated microsphere resonator were modeled using the finite element method via COMSOL Multiphysics. From the Electromagnetic Waves, Frequency Domain of Wave Optics in COMSOL, a 2D model for numerical simulation according to Maxwell's boundary conditions was adopted. To obtain fine simulations, the mesh size is set to 80 nm. A perfectly matched layer (PML) and scattering boundary conditions are employed as the external boundary of the model. The diameter of the microsphere cavity is set as 20 µm, with a thickness of surface CQWs increasing from 7 to 21 µm in steps of 7 µm to represent the increased number of CQW layers on the microsphere's surface. Refractive indices of silica microsphere, CQWs, and surrounding air are set as 1.45, 1.86, and 1.0, respectively. For the optical response from the 2D-3D microcavity configuration, 3D finite-difference time-domain simulations were done, employing a PML and scattering boundary conditions as the external boundary of the model. For ease of running simulations, the diameters of the microsphere and microfiber are reduced 20 times from 42 and 48 µm to 2.1 and 2.4 µm, respectively. Refractive indices of the silica microsphere, CQWs, and surrounding air are set as 1.45, 1.86, and 1.0, respectively.

Characterization Techniques—Steady-State PL, Absorption, and PL QY: For steady-state PL measurement, a homebuilt optical setup employing a He-Cd laser with excitation wavelength at 442 nm was used. Light signals were resolved and recorded with a monochromator with a diffraction grating of 600 groves per mm and equipped with a photon multiplier tube, using standard lock-in detection techniques to improve the signal-to-noise ratio. The measurement step was set as 0.2 nm. The absorption spectrum was measured using a Shimadzu RF-5301 PC spectrofluorometer with a measurement step of 0.5 nm. PL QY measurements were carried out by dispersing the CQW sample in hexane and placing it in an Otsuka Quantum Efficiency Measurement System QE2000, which consists of an integrating sphere optical system and monochromator integrated 150 W xenon lamp. The measurement was conducted using an excitation wavelength of 532 nm, the same as the excitation wavelength employed in subsequent nanosecond pulse excitation for lasing measurements.

Scanning Electron Microscopy: SEM characterization of microspheres before and after CQW coating and of uncoated core microfiber was conducted using JEOL JSM-7600F Schottky Field Emission Scanning Electron Microscope at an operating voltage of 5.0 kV under SEI (GB LOW) mode, and from the FESEM JEOL JSM-7800F PRIME at an operating voltage of 15.0 kV under SEM (LED) mode. EDS mapping was obtained from FESEM JEOL JSM-7800F PRIME.

Transmission Electron Microscopy: TEM characterization of core/shell CQWs was performed using a JEOL JEM 1400 Electron Microscope operating at 100 kV, with the colloidal CQW samples drop-casted on carbon-coated copper grids of 3.05 mm in diameter.

Measurement of Amplified Spontaneous Emission Spectra: For the optical pump source, a femtosecond amplified system producing 100 fs pulse width at an excitation wavelength of 400 nm of a 1 kHz repetition rate was employed. Pump-intensity-dependent edge emission was collected via a fiber-coupled spectrometer and detected by a silicon charged coupled device (CCD). The grating groove density was 600 groves per mm, and the spectrum resolution was 0.13 nm. A Thorlabs DCC1645C USB 2.0 CMOS microscopy camera was used for capturing an image of the spot size and subsequent calculations of spot size area for derivations of pump fluences from measured pump intensities.

Atomic Force Spectroscopy (AFM) and Surface Profiling of Flat Substrates: Atomic force spectroscopy and profiling of the surfaces of CQW-coated flat glass substrates were conducted using a Park NX10 atomic force microscope. Noncontact mode (NCM) was selected to study the surface of samples with a scan rate of 0.5 Hz. The scan area was limited to 5×5 μm^2 of a 1×1 cm^2 piece of sample substrate.

WGM Lasing Measurement and Setup: A homebuilt µ-PL system was employed to characterize lasing behavior from CQW-coated microsphere lasers and the 2D-3D microcavity configuration. For the excitation source, a 532 nm Q-switched Nd:YAG laser with a repetition rate of 60 Hz and pulse width of 1 ns was employed. The microsphere lasers or microcavity configuration were then placed on a 3D translation stage of an optical microscope, with optical signals collected from their top via a 50× (NA = 0.42) objective. The optical signals captured from the microspheres or microcavity configuration can then be transmitted to a camera for PL imaging or coupled to a spectrometer equipped with a silicon CCD camera of 0.043/0.019 nm spectral resolution for spectral recording and measurements.

PL Lifetime Measurements: Time-resolved PL measurements were conducted using a femtosecond amplified laser system with an excitation wavelength of 400 nm, 100 fs pulse width, and 1 kHz repetition rate. The PL signals were recorded with an Optronics streak camera having a temporal resolution of 50 ps.

Supporting Information

Supporting Information is available from the Wiley Online Library or from the author.

Acknowledgements

Y.T.T. and R.D. contributed to this work equally. This work was supported by the National Research Foundation of Singapore: NRF-CRP23-2019-0007 and AME-IRG-A20E5c0083. The SEM imaging and EDS mapping were performed at the Facility for Analysis, Characterization, Testing and Simulation (FACTS) at Nanyang Technological University, Singapore. H.V.D. and E.G.D. gratefully acknowledge the financial support in part from the Singapore Agency for Science, Technology and Research (A*STAR) MTC program under Grant No. M21J9b0085, Ministry of Education, Singapore, under its Academic Research Fund Tier 1 (MOE-RG62/20).

© 2023 Wiley-VCH GmbH

18638899, 2023, 7, Downloaded from https://onlinelibrary.wiley.com/doi/10.1002/lpor.202200849 by Bilkent University, Wiley Online Library on [10/07/2023]. See the Terms and Conditions (https://onlinelibrary.wiley.com/terms-and-conditions) on Wiley Online Library for rules of use; OA articles are governed by the applicable Creative Commons License

H.V.D. also gratefully acknowledges the support from TUBA. W.S.L. and C.X.X.L. acknowledge the support of EDB-IPP (REQ0165097).

Conflict of Interest

The authors declare no conflict of interest.

Data Availability Statement

The data that support the findings of this study are available from the corresponding author upon reasonable request.

Keywords

colloidal quantum wells, colloidal semiconductor microlasers, self-assembly, whispering-gallery-mode lasing

Received: November 9, 2022
Revised: February 1, 2023
Published online: March 9, 2023

[1] Z. Zhang, Y. T. Thung, L. Wang, X. Chen, L. Ding, W. Fan, H. D. Sun, *J. Phys. Chem. Lett.* **2021**, *12*, 9086.
[2] S. Ithurria, M. D. Tessier, B. Mahler, R. P. Lobo, B. Dubertret, A. L. Efros, *Nat. Mater.* **2011**, *10*, 936.
[3] S. Ithurria, B. Dubertret, *J. Am. Chem. Soc.* **2008**, *130*, 16504.
[4] M. Sharma, K. Gungor, A. Yeltik, M. Olutas, B. Guzelturk, Y. Kelestemur, T. Erdem, S. Delikanli, J. R. McBride, H. V. Demir, *Adv. Mater.* **2017**, *29*, 1700821.
[5] A. Dutta, A. Medda, S. Gosh, S. Sain, A. Patra, *ACS Appl. Nano Mater.* **2022**, *5*, 11679.
[6] Y. T. Thung, Z. Zhang, F. Yan, H. V. Demir, H. D. Sun, *Appl. Phys. Lett.* **2022**, *120*, 241105.
[7] B. Liu, Y. Altintas, L. Wang, S. Shendre, M. Sharma, H. D. Sun, E. Mutlugun, H. V. Demir, *Adv. Mater.* **2020**, *32*, 1905824.
[8] Z. Wen, P. Liu, J. Ma, S. Jia, X. Xiao, S. Ding, H. Tang, H. Yang, C. Zhang, X. Qu, B. Xu, K. Wang, K. L. Teo, X. W. Sun, *Adv. Electron. Mater.* **2021**, *7*, 2000965.
[9] C. She, I. Fedin, D. S. Dolzhnikov, A. Demortiere, R. D. Schaller, M. Pelton, D. V. Talapin, *Nano Lett.* **2014**, *14*, 2772.
[10] L. T. Kunneman, M. D. Tessier, H. Heuclin, B. Dubertret, Y. V. Aulin, F. C. Grozema, J. M. Schins, L. D. A. Siebbeles, *J. Phys. Chem. Lett.* **2013**, *4*, 3574.
[11] M. D. Tessier, C. Javaux, I. Maksimovic, V. Loriette, B. Dubertret, *ACS Nano* **2012**, *6*, 6751.
[12] M. Olutas, B. Guzelturk, Y. Kelestemur, A. Yeltik, S. Delikanli, H. V. Demir, *ACS Nano* **2015**, *9*, 5041.
[13] A. Naeem, F. Masia, S. Christodoulou, I. Moreels, P. Borri, W. Langbein, *Phys. Rev. B* **2015**, *91*, 121302.
[14] S. Delikanli, O. Erdem, F. Isik, H. D. Baruj, F. Shabani, H. B. Yagci, E. G. Durmusoglu, H. V. Demir, *J. Phys. Chem. Lett.* **2021**, *12*, 2177.
[15] B. Guzelturk, M. Pelton, M. Olutas, H. V. Demir, *Nano Lett.* **2019**, *19*, 277.
[16] N. Taghipour, S. Delikanli, S. Shendre, M. Sak, M. Li, F. Isik, I. Tanriover, B. Guzelturk, T. C. Sum, H. V. Demir, *Nat. Commun.* **2020**, *11*, 3305.
[17] S. Delikanli, F. Isik, F. Shabani, H. D. Baruj, N. Taghipour, H. V. Demir, *Adv. Opt. Mater.* **2021**, *9*, 2002220.
[18] B. Guzelturk, Y. Kelestemur, M. Olutas, S. Delikanli, H. V. Demir, *ACS Nano* **2014**, *8*, 6599.
[19] Y. Kelestemur, Y. Shynkarenko, M. Anni, S. Yakunin, M. L. D. Giorgi, M. V. Kovalenko, *ACS Nano* **2019**, *13*, 13899.
[20] Y. Altintas, K. Gungor, Y. Gao, M. Sak, U. Quliyeva, G. Bappi, E. Mutlugun, E. H. Sargent, H. V. Demir, *ACS Nano* **2019**, *13*, 10662.
[21] M. Wu, S. T. Ha, S. Shendre, E. G. Durmusoglu, W.-K. Koh, D. R. Abujetas, J. A. Sanchez-Gil, R. Paniagua Domiguez, H. V. Demir, A. I. Kuznetsov, *Nano Lett.* **2020**, *20*, 6005.
[22] R. Duan, Z. Zhang, L. Xiao, X. Zhao, Y. T. Thung, L. Ding, Z. Liu, J. Yang, V. D. Ta, H. D. Sun, *Adv. Mater.* **2022**, *34*, 2108884.
[23] J. Q. Grim, S. Christodoulou, F. D. Stasio, R. Krahne, R. Cingolani, L. Manna, I. Moreels, *Nat. Nanotechnol.* **2014**, *9*, 891.
[24] J. Yu, M. Sharma, M. Li, S. Delikanli, A. Sharma, M. Taimoor, Y. Altintas, J. R. McBride, T. Kusserow, T. C. Sum, H. V. Demir, C. Dang, *Laser Photonics Rev.* **2021**, *15*, 2100034.
[25] J. Maskoun, N. Gheshlaghi, F. Isik, S. Delikanli, O. Erdem, E. Y. Erdem, H. V. Demir, *Adv. Mater.* **2021**, *33*, 2007131.
[26] C. She, I. Fedin, D. S. Dolzhnikov, P. D. Dahlberg, G. S. Engel, R. D. Schaller, D. V. Talapin, *ACS Nano* **2015**, *9*, 9475.
[27] M. Li, M. Zhi, H. Zhu, W. Y. Wu, Q. H. Xu, M. H. Jhon, Y. Chan, *Nat. Commun.* **2015**, *6*, 8513.
[28] N. Gheshlaghi, S. Foroutan-Barenji, O. Erdem, Y. Altintas, F. Shabani, M. H. Humayun, H. V. Demir, *Nano Lett.* **2021**, *21*, 4598.
[29] Z. Yang, M. Pelton, I. Fedin, D. V. Talapin, E. Waks, *Nat. Commun.* **2017**, *8*, 143.
[30] Y. Gao, M. Li, S. Delikanli, H. Zheng, B. Liu, C. Dang, T. C. Sum, H. V. Demir, *Nanoscale* **2018**, *10*, 9466.
[31] S. Foroutan-Barenji, O. Erdem, S. Delikanli, H. B. Yagci, N. Gheshlagi, Y. Altintas, H. V. Demir, *Laser Photonics Rev.* **2021**, *15*, 2000479.
[32] M. Sak, N. Taghnipour, S. Delikanli, S. Shendre, I. Tanriover, S. Foroutan, Y. Gao, J. Yu, Y. Zhou, S. Yoo, C. Dang, H. V. Demir, *Adv. Funct. Mater.* **2020**, *30*, 1907417.
[33] K. J. Vahala, *Nature* **2003**, *424*, 839.
[34] S. M. Spillane, T. J. Kippenberg, K. J. Vahala, *Nature* **2002**, *415*, 621.
[35] A. Chiasera, Y. Dumeige, P. Feron, M. Ferrari, Y. Jestin, G. Nunzi Conti, S. Pelli, S. Soria, G. C. Righini, *Laser Photonics Rev.* **2010**, *4*, 457.
[36] Y. H. Lai, Y. K. Lu, M. G. Suh, Z. Yuan, K. J. Vahala, *Nature* **2019**, *576*, 65.
[37] C. Wang, X. F. Jiang, G. M. Zhao, M. Z. Zhang, C. Hsu, B. Peng, A. D. Stone, L. Jiang, L. Yang, *Nat. Phys.* **2020**, *16*, 334.
[38] P. J. Zhang, Q. X. Ji, Q. T. Cao, H. Wang, W. Liu, Q. Gong, Y. F. Xiao, *Proc. Natl. Acad. Sci. USA* **2021**, *118*, e2101605118.
[39] Q. T. Cao, R. Liu, H. Wang, Y. K. Lu, Y. F. Xiao, *Nat. Commun.* **2020**, *11*, 1136.
[40] P. Miao, Z. Zhang, J. Sun, W. Walasik, S. Longhi, N. Litchinitser, L. Feng, *Science* **2016**, *353*, 464.
[41] B.-B. Li, W. R. Clements, X.-C. Yu, K. Shi, Q. Gong, Y.-F. Xiao, *Proc. Natl. Acad. Sci. USA* **2014**, *111*, 14657.
[42] S. K. Özdemir, J. Zhu, X. Yang, B. Peng, H. Yilmaz, L. He, F. Monifi, S. H. Huang, G. L. Long, L. Yang, *Proc. Natl. Acad. Sci. USA* **2014**, *111*, E3836.
[43] R. Duan, X. Hao, Y. Li, H. Li, *Sens. Actuators, B* **2020**, *308*, 127672.
[44] T. Reynolds, N. Riesen, A. Meldrum, X. Fan, J. M. M. Hall, T. M. Monro, A. Francois, *Laser Photonics Rev.* **2017**, *11*, 1600265.
[45] M. Kuwata-Gonokami, S. Ozawa, R. H. Jordan, A. Dodabalapur, H. E. Katz, M. L. Schilling, R. E. Slusher, *Opt. Lett.* **1995**, *20*, 2093.
[46] T. J. Kippenberg, J. Kalkman, A. Polman, K. J. Vahala, *Phys. Rev. A* **2006**, *74*, 051802.
[47] V. D. Ta, R. Chen, H. D. Sun, *Adv. Opt. Mater.* **2014**, *2*, 220.
[48] V. D. Ta, R. Chen, H. D. Sun, *Sci. Rep.* **2009**, *9*, 17017.
[49] F. Luan, E. Magi, T. Gong, I. Kabakova, B. Eggleton, *Opt. Lett.* **2011**, *36*, 4761.
[50] J. Ward, O. Benson, *Laser Photonics Rev.* **2011**, *5*, 553.
[51] S. Yang, Y. Wang, H. D. Sun, *Adv. Opt. Mater.* **2015**, *3*, 1136.
[52] Y. Gao, M. C. Weidman, W. A. Tisdale, *Nano Lett.* **2017**, *17*, 3837.

 © 2023 Wiley-VCH GmbH

18638899, 2023, 7, Downloaded from https://onlinelibrary.wiley.com/doi/10.1002/lpor.202200849 by Bilkent University, Wiley Online Library on [10/07/2023]. See the Terms and Conditions (https://onlinelibrary.wiley.com/terms-and-conditions) on Wiley Online Library for rules of use; OA articles are governed by the applicable Creative Commons License

[53] B. Abécassis, M. D. Tessier, P. Davidson, B. Dubertret, *Nano Lett.* **2014**, *14*, 710.
[54] O. Erdem, K. Gungor, B. Guzelturk, I. Tanriover, M. Sak, M. Olutas, D. Dede, Y. Kelestemur, H. V. Demir, *Nano Lett.* **2019**, *19*, 4297.
[55] O. Erdem, S. Foroutan, N. Gheshlagi, B. Guzelturk, Y. Altintas, H. V. Demir, *Nano Lett.* **2020**, *20*, 6459.
[56] M. S. Khoskhoo, A. Prudnikau, M. R. Chashmejahanbin, R. Helbig, V. Lesnyak, G. Cuntiberti, *ACS Nano* **2021**, *15*, 17623.
[57] R. Momper, H. Zhang, S. Chen, H. Halim, E. Johannes, S. Yordanov, D. Braga, B. Blulle, D. Doblas, T. Kraus, M. Bonn, H. I. Wang, A. Riedimger, *Nano Lett.* **2020**, *20*, 4102.
[58] Y. S. Park, W. K. Bae, L. A. Padilha, J. M. Pietryga, V. I. Klimov, *Nano Lett.* **2014**, *14*, 396.
[59] Y. S. Park, W. K. Bae, T. Baker, J. Lim, V. I. Klimov, *Nano Lett.* **2015**, *15*, 7319.
[60] A. A. Rossinelli, H. Rojo, A. S. Mule, M. Aellen, A. Cocina, E. De Leo, R. Schäublin, D. J. Norris, *Chem. Mater.* **2019**, *31*, 9567.
[61] C. Reichardt, T. Welton, *Solvents and Solvent Effects in Organic Chemistry*, Wiley-VCH, Weinheim, Germany **2011**.
[62] M. Gomilšek, Whispering Gallery Modes, Vol. *11*, Univ. Ljubl. Ljubl. Semin **2011**, pp. 2-3.
[63] B. Guzelturk, M. Olutas, S. Delikanli, Y. Kelestemur, O. Erdem, H. V. Demir, *Nanoscale* **2015**, *7*, 2545.
[64] O. Erdem, M. Olutas, B. Guzelturk, Y. Kelestemur, H. V. Demir, *J. Phys. Chem. Lett.* **2016**, *7*, 548.
[65] R. Duan, Y. Li, H. Li, J. Yang, *Biomed. Opt. Express* **2019**, *10*, 6073.
[66] C. C. Lam, P. T. Leung, K. J. Young, *Opt. Soc. Am. B* **1992**, *9*, 1585.
[67] J. Hu, L. S. Li, W. Yang, L. Manna, L. W. Wang, A. P. Alivisatos, *Science* **2001**, *292*, 2060.
[68] L. Feng, Z. J. Wong, R. M. Ma, Y. Wang, X. Zhang, *Science* **2014**, *346*, 972.
[69] W. Liu, M. Li, R. S. Guzzon, E. J. Norberg, J. S. Parker, M. Lu, L. A. Coldren, J. Yao, *Nat. Commun.* **2017**, *8*, 15389.
[70] K. Rong, F. Gan, K. Shi, S. Chu, J. Chen, *Adv. Mater.* **2018**, *30*, 1706546.
[71] K. Oda, N. Takato, H. Toba, *J. Lightwave Technol.* **1991**, *9*, 728.
[72] G. Griffel, *IEEE Photonics Technol. Lett.* **2000**, *12*, 1642.
[73] Y. Y. Wang, C. X. Xu, M. M. Jiang, J. T. Li, J. Dai, J. F. Lu, P. L. Li, *Nanoscale* **2016**, *8*, 16631.
[74] K. Ge, J. Ruan, L. Cui, J. Tong, T. Zhai, *Opt. Express* **2022**, *30*, 28752.
[75] Y. Xiao, C. Meng, P. Wang, Y. Ye, H. Yu, S. Wang, F. Gu, L. Dai, L. Tong, *Nano Lett.* **2011**, *11*, 1122.
[76] K. Ge, D. Guo, B. Niu, Z. Xu, J. Ruan, T. Zhai, *Nanophotonics* **2021**, *10*, 4591.

© 2023 Wiley-VCH GmbH

18638899, 2023, 7, Downloaded from https://onlinelibrary.wiley.com/doi/10.1002/lpor.202200849 by Bilkent University, Wiley Online Library on [10/07/2023]. See the Terms and Conditions (https://onlinelibrary.wiley.com/terms-and-conditions) on Wiley Online Library for rules of use; OA articles are governed by the applicable Creative Commons License